molecular pharmaceutics

Article

pubs.acs.org/molecularpharmaceutics

Blood–Nanoparticle Interactions and *in Vivo* Biodistribution: Impact of Surface PEG and Ligand Properties

Neha B. Shah,[†] Gregory M. Vercellotti,[‡] James G. White,[§] Adrian Fegan,[∥] Carston R. Wagner,[∥] and John C. Bischof[*,†,⊥,#]

[†]Department of Biomedical Engineering, [‡]Department of Medicine, [§]Department of Lab Medicine and Pathology, [∥]Department of Medicinal Chemistry, [⊥]Department of Mechanical Engineering, and [#]Department of Urologic Surgery, University of Minnesota, Minneapolis, Minnesota 55455, United States

Supporting Information

ABSTRACT: Theranostic nanoparticles (NPs) cannot reach their target tissue without first passing through blood; however, the influence of blood protein and blood cell interactions on NP biodistribution are not well understood. The current work shows that 30 nm PEGylated gold NPs (GNPs) interact not only with blood proteins as thought before but also with blood cells (especially platelets and monocytes) *in vivo* and that longer blood circulation correlates strongly with tumor uptake. Further, GNP surface properties such as negative charge or lyophilization had either a minimal (i.e., charge) or 15-fold increase (i.e., fresh vs lyophilized) in blood retention times and tumor uptake. Tumor accumulation was increased over 10-fold by use of a bioactive ligand (i.e., TNF) on the lyophilized GNP surface. Resident macrophages were primarily responsible for the bulk of GNP uptake in liver while spleen uptake was highly surface property dependent and appears to involve macrophages and cellular interaction between the red and white pulp. This study shows that the PEG layer and ligand on the surface of the NP are critical to blood interactions and eventual tumor and RES organ biodistribution *in vivo*.

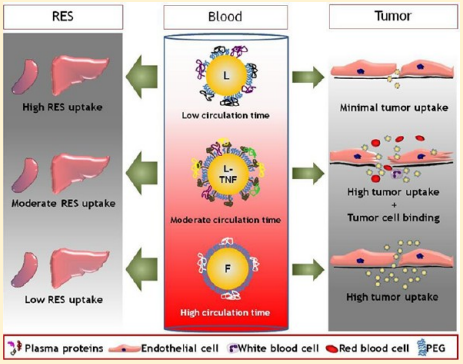

KEYWORDS: *gold nanoparticles, blood–particle interactions, biodistribution, ligand, PEGylation, lyophilization*

INTRODUCTION

Over the last three decades, reproducible synthesis, characterization, and modification techniques have significantly advanced the field of NP mediated detection, diagnostics, and therapeutics for numerous diseases including most notably cancer.[1] For instance, gold NPs (GNPs) now show promise in clinical trials as stand alone cancer therapeutics (Aurimmune) and as agents for photothermal therapies (AuroShell).[1−4] A large number of other GNP configurations (size, shape, surface chemistry, etc.) are currently being investigated in cell lines or preclinical model systems with the end goal of clinical application.[5] With increasing clinical opportunities there are also increasing concerns over GNP safety and regulation.[5−8] Thus to guide future work, more detailed understanding of GNP biodistribution *in vivo* is needed to support conditions of safe *in vivo* use and improve the effectiveness of the delivery to target sites (i.e., tumors). Historically, biodistribution studies on NPs such as liposomes have evaluated the blood circulation, organ distribution, and elimination kinetics of various NP configurations.[9,10] However, studies evaluating biological interactions of GNPs at the organ, tissue, and cellular level are infrequent and still in demand. Here, we show that blood–GNP interactions are critical in understanding *in vivo* biodistribution of GNPs with different surface chemistries.

Blood, which is largely composed of proteins and cells, is the first medium of contact for intravenously injected NPs. It is generally accepted that, when plasma proteins called opsonins bind to NPs in a process called opsonization, it results in the removal of NPs from blood circulation by the macrophages of the liver and spleen.[11] Since blood half-life of GNPs is known to impact their tumor accumulation,[12] it is important to determine the impact of blood–GNP interactions on GNP biodistribution. In addition to blood proteins, blood cells that make up 45% of blood volume can also interact with GNPs and contribute to their blood retention, elimination, and immunologic response. Recently, Bartneck et al. showed that primary human monocytes and monocyte derived cells take up large quantities of spherical and rod shaped GNPs *in vitro*.[13] It is likely that such uptake can occur *in vivo*, but it has yet to be demonstrated to our knowledge.

Blood retention of GNPs can be strongly influenced by their surface chemistry such as PEG coating, charge, and ligand.[12] However, tumor accumulation remains consistently below 5% of injected dose (ID), and liver and spleen accumulation remain consistently high regardless of GNP physicochemical properties. Furthermore, it has been shown that GNPs distribute within tumor tissue based on their size and tumor cell binding

Received: December 7, 2011
Revised: April 24, 2012
Accepted: June 1, 2012
Published: June 5, 2012

Table 1. Characterization of GNPs

name	hydrodyn diam (nm)	charge (mV)	SH-PEG	PEG MW	ligand	charge	storage	source
L-GNP	60.2 ± 2.0	−10.6 ± 2.6	$-CH_3$	5000	N/A	neutral	lyophilized	CytImmune Sciences, Inc.
L-GNP^{TNF}	71.7 ± 5.7	−2.9 ± 0.6	$-CH_3$	5000	TNF-α	neutral	lyophilized	
F-GNP	66.50 ± 0.79	−2.6 ± 1.5	$-CH_3$	5000	N/A	neutral	suspension in DI water	Bischof lab[a]
F-GNP$^-$	62.83 ± 0.06	−27.1 ± 5.2	−COOH	5000	N/A	negative	suspension in DI water	

[a]GNP synthesis protocols were obtained from the laboratory of Dr. Warren Chan at the University of Toronto.

only occurs when a targeting ligand is present.[12,14−16] In liver, the uptake of GNPs appears to be dominated by Kupffer cells (a resident macrophage) with potential clearance by hepatobiliary system.[17] In spleen, TEM studies have also shown the uptake of GNPs in macrophages;[14,18] however, the spleen is a more complex organ with multiple types of phagocytic cells and TEM is not expected to fully elucidate the biodistribution and cellular uptake. Thus, a more careful study that links the blood interactions of NPs with organ distribution over time is needed.

The present work examines the effect of surface properties on the biological interactions of GNPs in tumor bearing mice. Blood cell interactions were studied using TEM, and tissue interactions were studied using histology. We also performed quantitative biodistribution over time to correlate the biodistribution of GNPs in blood, tumor, liver, and spleen.

RESULTS AND DISCUSSION

Four GNPs with identical core size, but varying surface properties including fresh (F-GNP) and lyophilized PEG (L-GNP), charge (F-GNP$^-$), and bioactive ligand (L-GNP^{TNF}), were tested as shown in Table 1. All four GNPs were characterized for their size, aggregation, and surface charge by dynamic light scattering (DLS), UV−vis spectroscopy, and zeta potential measurement respectively. The results of the characterization are included in Table 1, Supplementary Table T1 in the Supporting Information, and Supplementary Figures S1 and S2 in the Supporting Information. The amount of gold in each tissue at a given time point is plotted in Figure 1 as a percentage of the injected dose per ml of blood or gram of tissue (% ID/ml or % ID/g). Figure 2 shows the blood cell−GNP interaction TEM results. Figures 3, 4, and 5 show the histology of tumor, liver, and spleen respectively corresponding to the time points displayed for quantitative data in Figure 1 (A − E).

Blood Biodistribution: Blood Protein and Blood Cell−GNP interactions. The use of fresh vs lyophilized PEG and a bioactive ligand, TNF, were two major contributors to longer blood circulation times for the GNPs tested, whereas negative charge was found to be less important. As a first test of GNP−blood interactions a complement activation assay for each GNP in Table 1 was performed. The result for the ELISA of C3a on plasma from animals treated with each GNP compared to untreated controls is shown in Figure 1F. While there is some variation, we were unable to measure a statistically significant change in complement activation after GNP blood exposure *in vivo* (Figure 1F). This agrees with the literature on this subject, which suggests that no major complement activation occurs with PEGylated GNPs.[19] It is therefore presumed that the biodistribution behavior discussed below is predominantly independent of complement activation.

The fresh PEG and TNF GNPs stayed in the blood circulation the longest while the lyophilized GNP was quickly cleared from the blood. Blood concentration of GNPs was measured at specified time points and reported as % ID/mL or % ID/g. At 1 h, the concentration of GNPs in circulating blood is approximately 40% ID/mL for all but L-GNP. F-GNP showed high blood retention at 1 and 8 h (45.84 and 34.05% ID/mL respectively) and was still present in blood in detectable quantities at 24 h (Figure 1A). Contrary to this, L-GNP was only measurable in blood at 1 h at 3.86% ID/mL and below the detection limit thereafter (Figure 1A). A major difference between the two GNPs is that F-GNP is freshly synthesized and stored in a solution form, whereas L-GNP is lyophilized for long-term storage. Though the core size of both particles is similar (30 nm), their hydrodynamic diameter is different. It is possible that the process of lyophilization has an adverse effect on the surface PEG coverage of L-GNP. As shown in Table 1, the zeta potential (surface charge) of L-GNP is slightly negative (−10.6 ± 2.6 mV), suggestive of incomplete surface coverage by PEG, because complete surface coverage results in close to neutral surface charge (−2.6 ± 1.5 mV for F-GNP). Thus, lyophilization potentially results in partial PEG coat stripping. Previously reported studies suggest that fragmented PEG coating on a NP surface can lead to their opsonization by plasma proteins,[20,21] formation of protein-NP aggregates,[22] and finally nonspecific uptake by macrophages *in vitro*[23] or *in vivo* in RES organs.[24] For instance, Fibrinogen is the most abundant of serum proteins to bind 30 nm bare (i.e., non-PEGylated) GNPs[19] which upon binding can expose the $\gamma^{377-395}$ chain[25] allowing the protein−NP complexes to be recognized and phagocytosed by macrophages and leukocytes.[25] This is one of the possible mechanisms for the faster clearance of L-GNP from blood circulation.

By simply adding a bioactive ligand, TNF, to L-GNP its biodistribution can be dramatically changed. Specifically, L-GNP^{TNF} showed an order of magnitude higher retention in blood at 1 h compared to L-GNP (31.62% vs 3.86% vs ID/mL, Figure 1A). We speculate that this is due to the presence of the TNF-α on its surface, which alters the interactions of these particles with blood components such that they are not as readily cleared by the RES system. Concentration of L-GNP^{TNF} drops in blood by 50% from 1 to 8 h and to 0.52% ID/mL at 24 h. The increase in the blood circulation time correlates strongly with accumulation in tumor that increases significantly from 0.71 to 1.97% ID/g from 1 to 8 h, and further to 3.38% ID/g at 24 h. None of the other GNPs showed significant increase in the tumor accumulation from 8 to 24 h. This strongly suggests that the blood retention of L-GNP^{TNF} is mediated in part by the bioactivity of TNF-α on the lyophilized particles as previously suggested.[18,26]

Charge was also found to be a mediator, albeit far less than TNF, for blood−GNP interaction. Specifically, the blood concentration of F-GNP$^-$ is comparable to that of F-GNP at 1 h (43.46% vs 45.84% ID/mL respectively), but F-GNP$^-$ is cleared more efficiently at later time points (8 and 24 h). As can be seen in Table 1, the most important difference between these two particles is the negative surface charge on F-GNP$^-$,

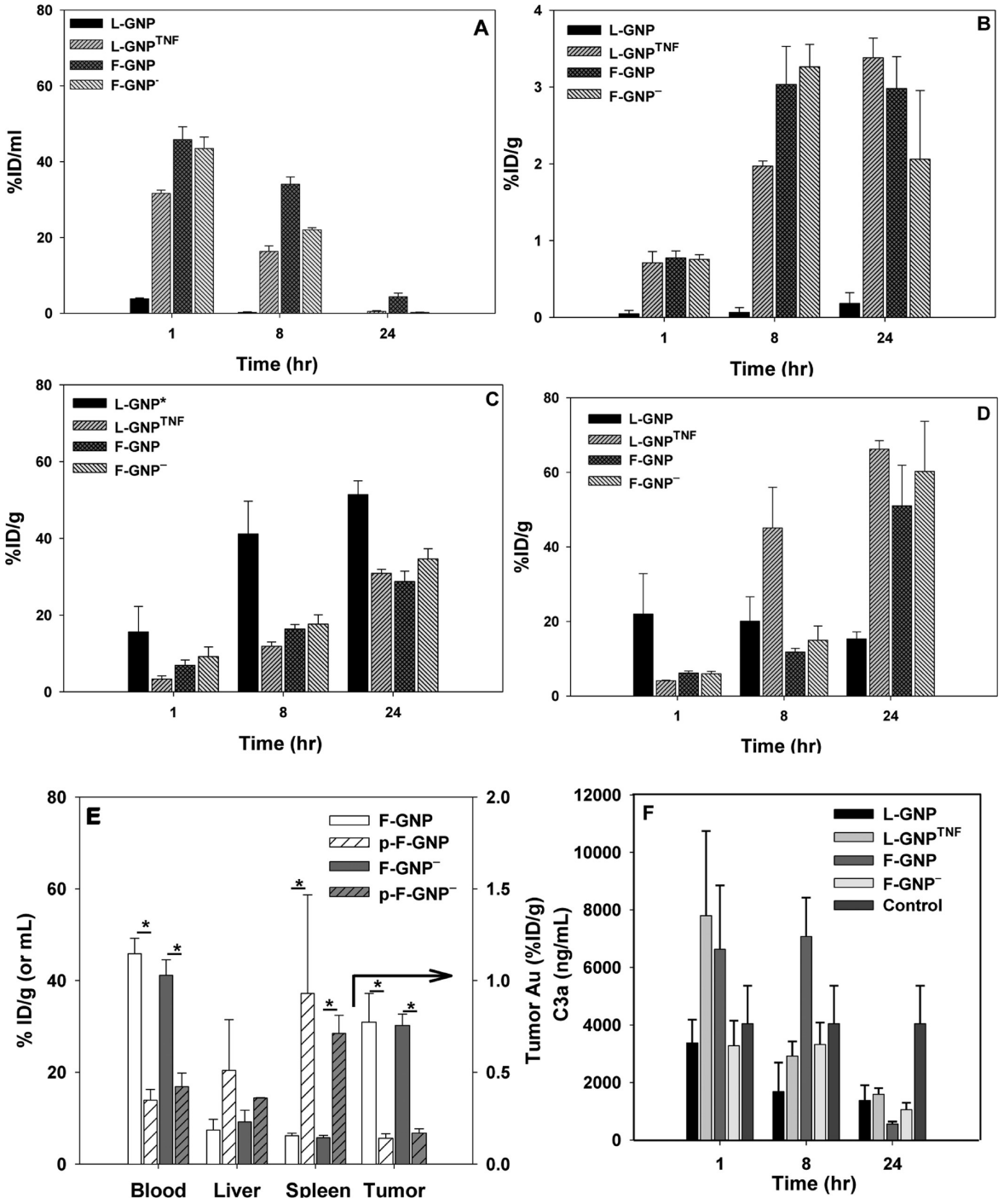

Figure 1. Quantitative *in vivo* organ distribution of intravenously injected GNPs in (A) blood; (B) tumor; (C) liver; (D) Spleen. Blood, tumor, liver, and spleen accumulation of GNPs varied based on their surface properties. ICP-MS (blood) and ICP-AES (other organs) were used for quantitative analysis. L-GNP* is 27 nm in core diameter as supplied by CytImmune Sciences, Inc. (E) Biodistribution of plasma sensitized GNPs. GNPs were incubated with mouse plasma before injection (p-F-GNP, p-F-GNP$^-$). Gold concentration is measured 1 h postinjection. * indicates significant difference of p-GNPs from F-GNPs. (F) Complement activation. No significant differences were observed between control and treated animals for C3a activation. Control animals were not treated with any GNPs. Accumulation is indicated as a percentage of injected dose (% ID/g tissue). Data are given in mean ± SEM, n = 3−5. Statistical significance, $p < 0.05$.

due to the carboxylic end group on PEG. It has been shown that, for small NPs, the PEG chains assume parabolic shape due to the high surface curvature which prevents the end group from being exposed to the blood proteins.[13,27] If this is the case, F-GNP and F-GNP$^-$ would appear as the same particle to blood proteins, which would explain the similar blood concentration at 1 h. Moreover, preincubation with mouse plasma also does not alter the blood retention of F-GNP and F-GNP$^-$ from each other (Figure 1E), which suggests that the protein corona of both of these particles may be similar. The faster clearance of F-GNP$^-$ at later time points may be because of the eventual exposure of the carboxylic acid end group leading to opsonization. While F-GNP has a higher retention than F-GNP$^-$, it is also mostly removed from blood by 24 h

dx.doi.org/10.1021/mp200626j | *Mol. Pharmaceutics* 2012, 9, 2146−2155

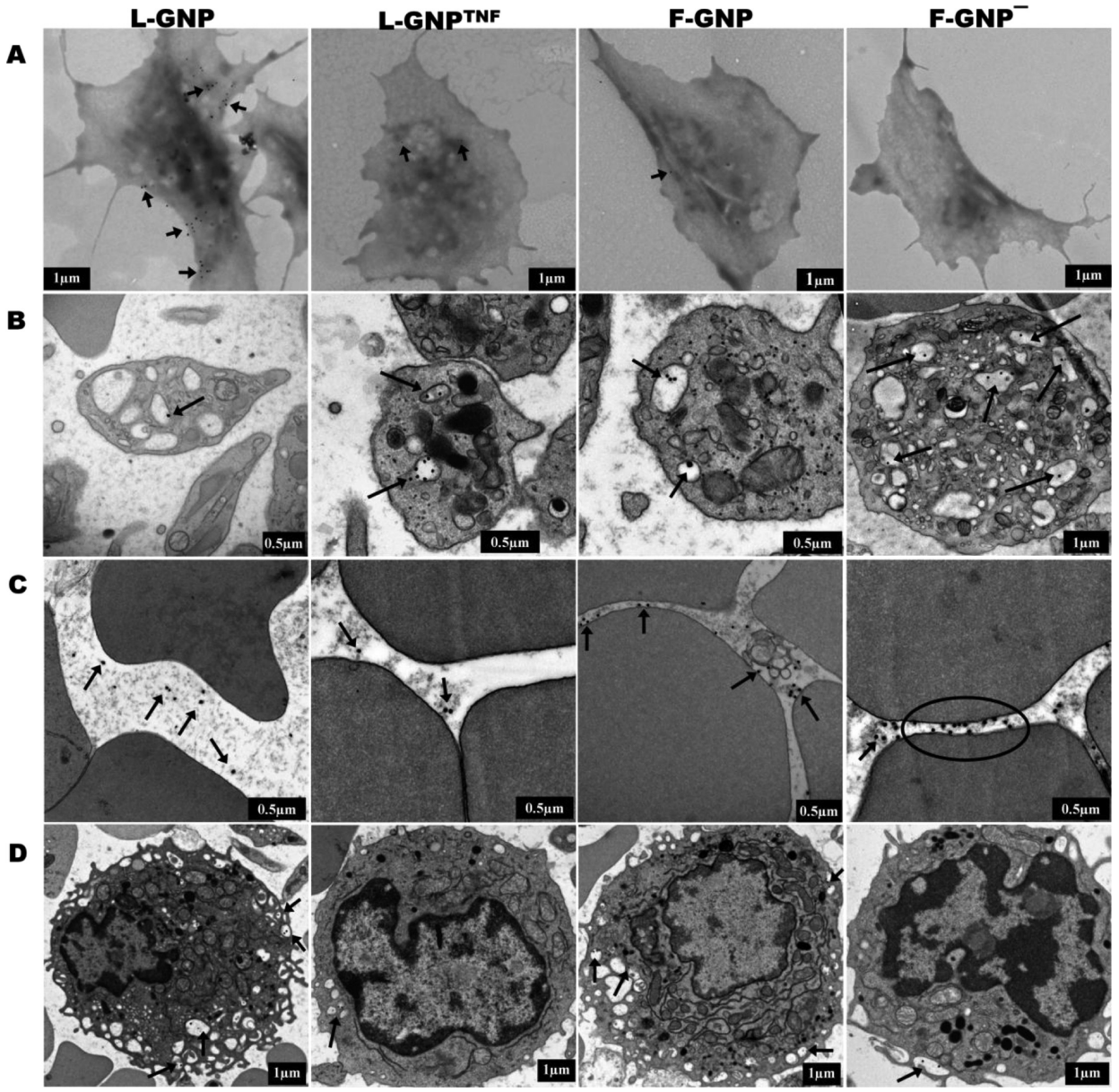

Figure 2. TEM imaging of GNP–blood cell interaction *in vitro* and *in vivo*. TEM micrographs of blood cells *in vitro* (A), or *in vivo* (B–D) post-GNP exposure. (A) GNPs bind to the surface of washed platelets after 15 min of incubation. L-GNP shows highest binding, and F-GNP^{-} shows no binding. (B) Circulating platelets show GNP uptake in OCS 1 h postinjection in tumor bearing mice. (C) Except for F-GNP^{-} circulating RBCs show no interactions with GNPs. F-GNP^{-} bind to the RBC surface membrane. (D) All GNPs show uptake in circulating blood monocytes. GNPs are located in small vacuoles, a characteristic of monocytes. Black arrows indicate GNP localization.

(<5% remaining) likely due to the eventual protein binding to PEG chains, or the degradation of PEG layer over time in circulation leaving all GNPs vulnerable to opsonins.

NP–blood protein interaction (opsonization) may play an important role in the clearance of NPs from the blood circulation as already mentioned. Opsonization of GNPs can also lead to their recognition and binding/uptake by circulating blood cells. These GNP loaded circulating blood cells can then either leave the circulation to reside in one of the RES organs or be removed from the circulation by the macrophages of RES organs. Recent *in vitro* studies have shown that primary human blood monocytes, neutrophils, and monocyte derived macrophages take up GNPs in *in vitro* culture.[13,28,29] Our *in vitro* study with mouse blood showed similar results (Supplementary Figure S4 in the Supporting Information). However, the arguably more important question of whether there are *in vivo* interactions between GNPs and blood cells is a relatively unexplored topic to which our results below contribute.

Blood Cell–GNP interaction *in Vitro* and *in Vivo*. TEM analysis of blood–GNP interactions reveals that GNPs can interact with platelets, red blood cells (RBCs), and white blood cells (WBCs) both *in vitro* and *in vivo*. Interactions with mouse platelets are shown in Figure 2A,B, RBCs in Figure 2C, and WBCs in Figure 2D (and Supplementary Figure S5 in the Supporting Information). *In vitro*, L-GNP binds to platelets in large numbers, L-GNP^{TNF} and F-GNP show some binding, and F-GNP^{-} shows no binding at all (Figure 2A). SEM analysis showed that GNPs not only attached to the platelet surface but were buried in small grooves inside the cell membrane suggestive of the open canalicular system (OCS)[30] (Supple-

dx.doi.org/10.1021/mp200626j | *Mol. Pharmaceutics* 2012, 9, 2146–2155

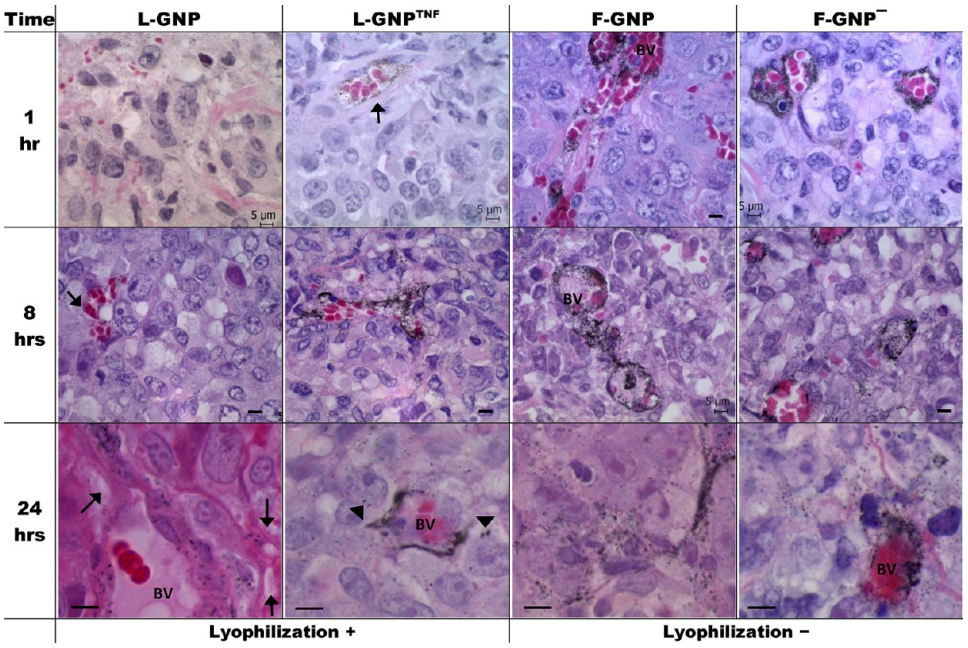

Figure 3. Histological analysis of GNP tumor distribution over time. Light micrographs of silver enhanced tumor sections show GNP accumulation/distribution changes over time with the type of GNP used. H&E counterstain allows identification of various features of the tissue, including blood vessels. GNPs mainly accumulate around blood vessels (BV) at 1 and 8 h, and distribute away from BV at 24 h. Silver enhanced GNPs show up as black dots (indicated with arrows where not obvious). Enlarged images at 24 h show the spreading of GNPs around BV. Arrowheads indicate GNP binding to tumor cells. [Scale bar = 5 μm unless indicated otherwise.]

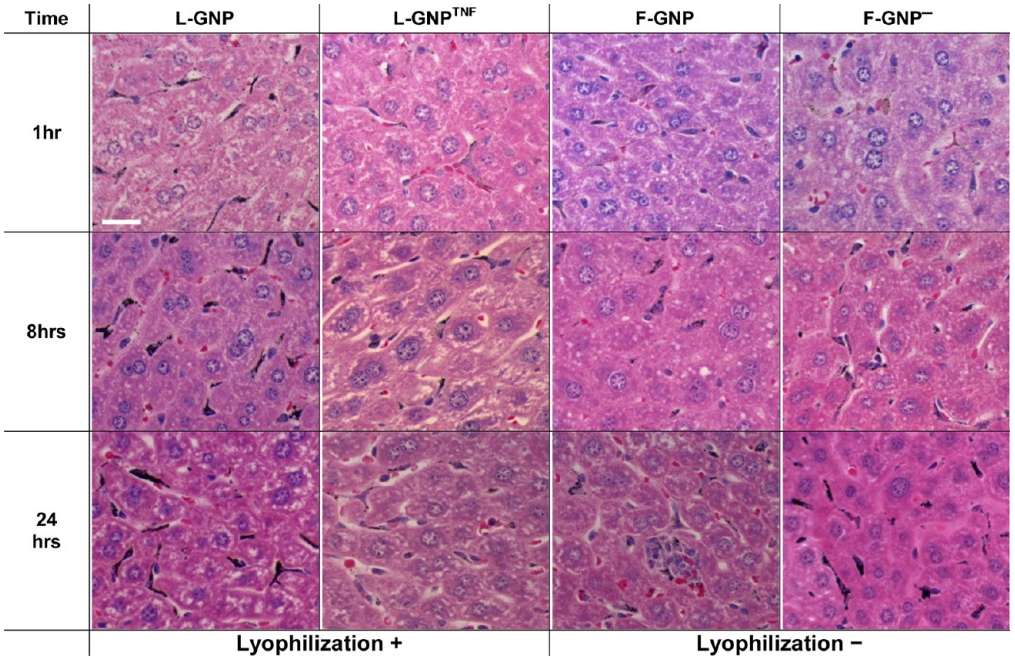

Figure 4. Histological analysis of GNP liver distribution over time. Light micrographs of silver enhanced liver sections show GNP accumulation/distribution changes over time with the type of GNP used. Sections were counterstained with H&E for identification of various features of the tissue. Silver enhanced GNPs show up as black dots. GNPs mainly accumulate in Kupffer cells with rare binding to hepatocytes at 24 h. L-GNP shows highest and F-GNP shows the least accumulation at all time points. Kupffer cells stain completely black in L-GNP condition due to high uptake of GNPs. L-GNP^{TNF} and F-GNP^{-} show similar distributions, which increase over time. [Magnification = 40×, scale bar = 20 μm.]

mentary Figure S4 in the Supporting Information). *In vivo* platelet analysis 1 h postinjection showed that all GNPs were taken up in platelets as shown in Figure 2B. Again, single or multiple GNPs were found inside hollow vacuoles which appear to be part of the platelet OCS.[31] Interestingly, F-GNP^{-}, which did not show any binding to the platelets *in vitro*, also showed uptake in the circulating platelets. This suggests that the GNP uptake in platelets *in vivo* is nonspecific and perhaps mediated by protein−GNP interactions. This result also suggests that *in vitro* studies of blood cell−GNP interactions may not provide an accurate model of their *in vivo* interaction behavior. Interestingly, the platelets showing uptake of GNPs did not

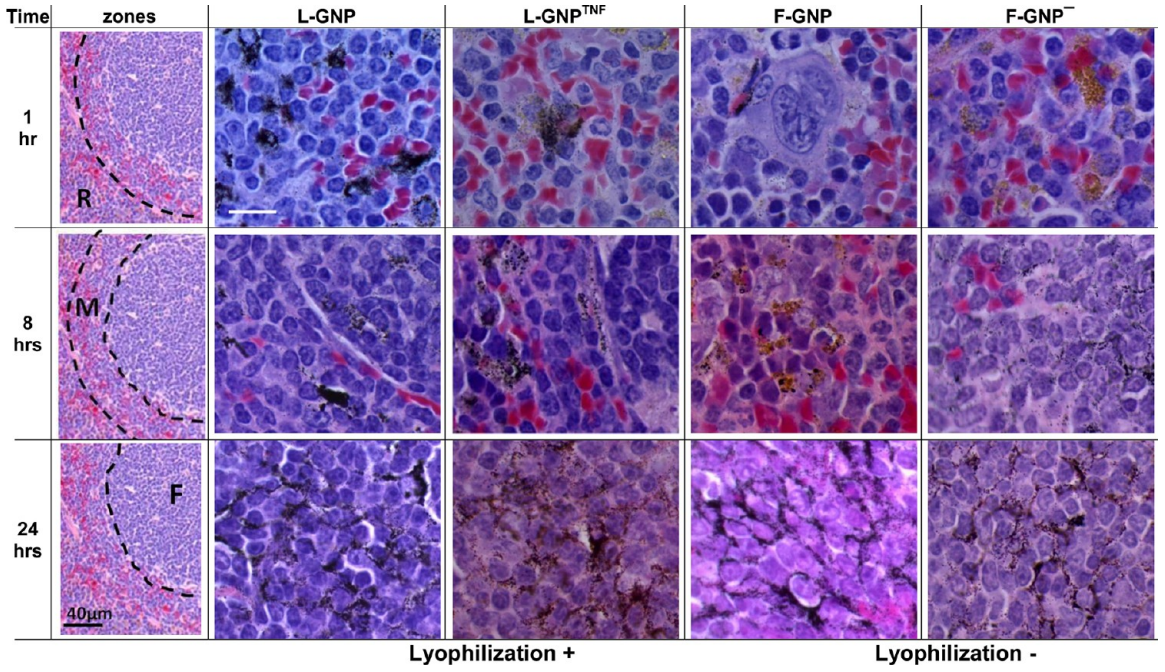

Figure 5. Histological analysis of GNP spleen distribution over time. Light micrographs of silver enhanced spleen sections show GNP accumulation/distribution changes over time with the type of GNP used. Sections were counterstained with H&E for identification of various features of the tissue. Silver enhanced GNPs show up as black dots. The distribution of GNPs shifts from red-pulp (R) to follicular regions (F). "Anatomical zones" show where majority of GNPs are located at each time point, and the corresponding row shows high magnification image for each particle of that zone. Images were acquired at 100×. R, red pulp; M, marginal zone; F, follicle. [Scale bar = 10 μm unless indicated otherwise.]

show loss of granules, a sign of platelet activation since activated platelets release their granules extracellularly. Additionally, if GNPs acted as platelet activators, then platelets would undergo shape induced aggregation and release of ATP (from granules), which in our hands using mouse blood did not occur (data not shown). Thus, it is not clear at this point how the uptake of GNPs in the platelets affects platelets although there is evidence to suggest that particle uptake in platelets leads to their downstream phagocytosis by macrophages.[32] In short, circulating platelets can partake in the removal of NPs from the bloodstream but neither platelets nor the complement system appears to be activated by these GNPs. Further blood cell types are explored below.

GNPs in this study, with the exception of F-GNP$^-$, did not show any binding or uptake in RBCs *in vivo* (Figure 2C). While we were able to demonstrate GNP−RBC membrane association *in vitro*, definitive binding or uptake was not conclusively measured (data not shown). The RBC is the most abundant cell type in the circulating blood, and there has been a great deal of interest in attaching NPs to the RBC surface to increase NP blood circulation time.[33,34] Zhao et al. recently showed that NPs bind to RBCs in a size dependent manner and cause deformation of the surface membrane in some cases.[35] Another *in vitro* study showed that NP binding to RBCs can also result in their uptake into the RBC cytoplasm.[36] The occasional binding of F-GNP$^-$ to RBC surface membrane *in vivo* was shown by TEM in (Figure 2C) and confirmed using SEM (Supplementary Figure S4 in the Supporting Information). If this generates any RBC membrane damage, it may lead to an increase in spleen uptake due to damaged RBCs recycling.

In contrast to RBCs, WBCs, especially monocytes, clearly showed uptake of all GNPs regardless of their surface properties *in vivo* as shown in Figure 2D and also *in vitro* (Supplementary Figure S5 in the Supporting Information). Monocytes, as determined by TEM ultrastructure, show GNPs in different stages of the uptake. For example, F-GNP$^-$ are wrapped in membrane pseudopodia (Figure 2D F-GNP$^-$). L-GNPs are found in pseudopodia as well as vacuoles that formed after the pseudopodia merged with the membranes. L-GNP^{TNF} and F-GNP are located in membrane bound vesicles that look like phagolysosomes. Additionally, we noticed some uptake of GNPs in neutrophils as well, but none in lymphocytes. This is consistent with our *in vitro* data in mouse blood cells (Supplementary Figure S5 in the Supporting Information) and previous *in vitro* studies conducted in primary human blood cells.[13]

Tumor Biodistribution. Tumor accumulation of GNPs generally increases with increased blood circulation time.[12] As noted above blood circulation times are positively impacted by the use of fresh PEG and a bioactive ligand (TNF). In this section, we demonstrate that tumor accumulation is likewise positively impacted for these same particles although never exceeding 3−4% ID/g tissue by ICP-AES (Figure 1B). Specifically, accumulation of L-GNP was negligible (<0.5% ID/g) in tumor at all times possibly due to their poor blood retention (Figure 1B). However, L-GNP^{TNF} shows measurable accumulation in tumor (0.71%, 1.97%, and 3.38% ID/g at 1, 8, and 24 h) due to the initial high concentration in blood. F-GNP and F-GNP$^-$ show high tumor accumulation at all times because of longer blood retention (Figure 1B). For example, at 8 h 3.03% ID/g of F-GNP and 3.26% ID/g of F-GNP$^-$ were found in tumor. In order to probe the vascular vs interstitial accumulation, further histology was performed.

Figure 3 shows histological sections of tumor from mice treated with GNPs. Silver enhancement of tissue sections allows selective precipitation of silver on GNPs, thus making them large enough to be visualized by light microscopy. Consistent with quantitative analysis, L-GNPs were not easily

found in the tumor at 1 h; however, some accumulation was observed at later time points in the vasculature. F-GNP and F-GNP^{-} showed noticeable accumulation around blood vessels even at 1 h; however, at this stage particles remained confined to the vasculature. The migration of particles away from blood vessels and into the extracellular matrix (ECM) at 8 h was only noticeable at high magnification. At 24 h, there was a noticeable spread of GNPs in the ECM. Perrault et al. have demonstrated that smaller particles show higher migration away from the blood vessels into the tumor matrix beginning around 8 h postinjection, whereas 60 nm GNPs (hydrodynamic diameter) that are comparable in size to the GNPs tested here show moderate migration from the blood vessels.[12] Though we did not see much migration of GNPs from blood vessels at 8 h, at 24 h all GNPs showed scattered distribution around blood vessels.

The addition of a bioactive ligand (TNF) increases the tumor biodistribution of L-GNP by an order of magnitude (0.18% ID/g L-GNP vs 3.38% ID/g L-GNP^{TNF}) by a combination of cellular and vascular (i.e., EPR) mechanisms. Previously transferrin and EGFR coated GNPs have been shown to specifically bind to tumor cells 24 h after intravenous injection by histology, while untargeted GNPs did not.[15,16] In this study, L-GNP^{TNF} also showed some binding to the tumor cells in the interstitial space beyond the vasculature as indicated with arrowheads in Figure 3, possibly due to the binding of TNF-α to its receptors on tumor cells (Figure 3 L-GNP^{TNF}). Interestingly, this suggests tumor accumulation of L-GNP^{TNF} was first achieved by extravasation and secondarily by TNF binding. However, while always significantly greater than L-GNP, the tumor accumulation of L-GNP^{TNF} remained initially lower (1−8 h) compared to F-GNP and F-GNP^{-} only catching up to over 3% ID/g at 24 h. This leads us to believe that the TNF-α is interacting directly with the tumor vasculature, resulting in vascular hyperpermeability (EPR manipulation) which in turn increases GNP tumor accumulation.[37,38] Clearly an important future study will be the creation of an F-GNP^{TNF} which will presumably enhance blood circulation and tumor accumulation even further.

RES Organs. Consistent with previous biodistribution studies, we found that the majority of GNPs accumulate in liver and spleen after iv injection, regardless of their surface properties (Figure 1C,D). However, the accumulation tends to vary based on NP surface properties. Specifically, fresh PEG and TNF yield roughly 30% ID to liver and 60% ID to spleen whereas lyophilized PEG led to 50% in the liver and only 15% in the spleen. Interestingly, the same three particles that avoid the liver also load best within the tumor. The following two sections discuss quantitative and histological results specific to this biodistribution.

Liver Biodistribution. Regardless of their physicochemical parameters, all GNPs accumulate in liver in large quantities (28−51% ID/g at 24 h.). We have previously demonstrated that PEGylated GNPs (L-GNP in this study) show higher uptake in liver from 0 to 4 h compared to GNP with TNF (L-GNP^{TNF} in this study).[18] This study also suggests that L-GNP accumulation is significantly higher compared to L-GNP^{TNF}, F-GNP, and F-GNP^{-} at 8 and 24 h (p-value <0.05). By 24 h, 51.37% of L-GNP is found in liver compared to 28.75% of the F-GNP. Liver histology indicates that the accumulation is predominantly phagocytic uptake by Kupffer cells, which is in agreement with literature.[15−17,39] In addition, L-GNP shows stronger silver staining in Kupffer cells at 1 h compared to all other GNPs, which agrees with the higher quantitative accumulation in liver in Figure 1. This suggests a deficiency in the PEG layer increases opsonization and uptake by liver macrophages. Accumulation of L-GNP^{TNF} and F-GNP^{-} also increase with time, but never reaches the same state as L-GNP. Livers of animals treated with F-GNP stain light at all time points, which is also in agreement with quantitative measurements in Figure 1C. Importantly, occasional binding and uptake in hepatocytes was observed. For instance, L-GNP^{TNF}, F-GNP, and F-GNP^{-} showed some binding and uptake by hepatocytes at 1 h (data not shown). However, by 8 h such binding was not observed. Hardonk et al. tested liver accumulation with 17 and 79 nm albumin and PVP coated gold particles and showed that only the 17 nm particles were detected in the hepatocytes.[17] This suggests the possibility that the 30 nm particles tested here are in the range where hepatocyte interaction decreases. In some cases GNP binding to endothelial cells was also observed but was not considered significant (data not shown). Additionally, circulating WBCs also showed NP uptake/attachment in larger blood vessels of the liver, which complements the blood cell TEM data (Figure 2D) (data not shown).

Spleen Biodistribution. In contrast to the liver, GNP accumulation in spleen involves multiple cell types and is highly surface chemistry dependent, loading close to 60% ID/g by 24 h for most GNPs, but never rising above 15% ID/g for L-GNP. For example, as the concentration of F-GNP dropped in blood from 34.05% ID/mL at 8 h to 4.35% ID/mL at 24 h, the accumulation in spleen significantly increased from 11.78% ID/g to 51.03% ID/g (Figure 1D). A similar but earlier change is observed for L-GNP^{TNF}, where an approximately 50% drop in blood concentration from 1 to 8 h is followed by a sudden increase in its accumulation in spleen (4.10−45.08% ID/g from 1 to 8 h, Figure 1D). Though the accumulation of L-GNP^{TNF} in liver also increases from 3.35% ID/g to 11.88% ID/g (from 1 to 8 h), this change is not as dramatic as it is in the spleen. Interestingly, the concentration of L-GNP in spleen does not change significantly over all times tested, remaining consistently between 15 and 20% ID/g.

Histological analysis in Figure 5 shows that GNP accumulation in spleen occurred in one or more of the three anatomical zones of the spleen. Zone R refers to the red pulp (red cell filtration), zone F refers to the white pulp (houses lymphocytes), and zone M refers to the marginal zone (interface between zones R and F). By 1 h, most GNPs show accumulation in zone R but not other zones. At 8 h, accumulation of all GNPs was also found in zone M in addition to zone R with F-GNP^{-} even showing some accumulation in zone F. After 24 h all GNPs showed accumulation in zone F as well. To our knowledge such observations regarding the shifting biodistribution of GNPs in different zones of splenic anatomy over 24 h have not been made before.

Unlike liver, the basic histological analysis of spleen does not clearly identify the cell types involved in the uptake of GNPs. The spleen hosts a number of cell types in addition to the macrophages including reticular cells, lymphocytes, and a variety of dendritic cells. We believe that the numerous macrophages in zone R take up the GNPs at the initial time point (1 h). However, the migration to zone M (8 h) and zone F (24 h) likely also involves dendritic cells (DC) that express MAC-1 receptors,[40] which can recognize the fibrinogen−GNP complexes as discussed above. Importantly, the mechanism by

which any of these cells recognize and take up GNPs at 24 h is not yet clear. Immunohistochemical analysis of these sections may help explain these phenomena. Our results show that the biodistribution of GNPs in spleen may involve more than one cell type and a complex interplay among these cells.

Plasma Sensitization: Altered RES and Tumor Uptake. Finally, plasma sensitization (one test of opsonin exposure and RES removal) of the two freshly PEGylated GNPs was found to increase accumulation in spleen while leaving liver uptake unaltered and ultimately reducing tumor uptake (Figure 1E). This test was performed by incubating the GNPs with mouse plasma before injecting them in tumor bearing mice. Blood retention of plasma sensitized GNPs (p-F-GNP and p-F-GNP$^-$) while comparable to each other was found to be significantly lower compared to F-GNP and F-GNP$^-$ (Figure 1E) at 1 h. In accordance with this, the accumulation of plasma sensitized GNPs in tumor was approximately 5-fold lower compared to F-GNP and F-GNP$^-$. Interestingly, while the liver accumulation of plasma sensitized GNP remained unchanged compared to nonsensitized GNPs, the spleen accumulation of p-F-GNP and p-F-GNP$^-$ was significantly higher (37.18 and 28.48% ID/g respectively) compared to F-GNP and F-GNP$^-$ (6.19 and 5.74% ID/g respectively). Collectively these results suggest that mouse plasma yields a similar protein corona on F-GNP and F-GNP$^-$, thereby allowing similar biodistribution trends. Additionally, it may be that the accumulation of GNPs in liver is independent of the plasma protein binding on the GNP surface. Nevertheless, plasma sensitization significantly alters spleen accumulation. Thus, we believe that the protein corona contains proteins that mediate uptake of these particles by certain cell types in spleen. A detailed further investigation in this area is warranted.

CONCLUSION

In summary, our results demonstrate that GNPs show binding and uptake interactions with blood cells including platelets, RBCs, and WBCs *in vivo*. GNPs are taken up in circulating platelets and WBCs (i.e., monocytes) regardless of their surface properties. Our data also suggests that tumor accumulation of GNPs is governed by tumor physiology or vascular leak; hence, the longer the particle remains in circulation, the higher the accumulation in tumor. Blood retention of GNPs was strongly affected by their surface properties, especially the PEG coverage and ligand. It was also demonstrated that Kupffer cells are central to removal of GNPs from circulation in liver; however, in the spleen multiple cell types and their interactions create a shifting pattern of GNP uptake over time within different splenic anatomic zones.

MATERIALS AND METHODS

Gold Nanoparticles. *In vivo* studies were performed with four GNPs that are divided into two groups. The first group consisted of previously synthesized, PEGylated, and lyophilized GNPs with and without a bioactive ligand (TNF-α) from an industrial source (L-GNP and L-GNP^{TNF}) (CytImmune Sciences, Inc.). Each 1 μg of gold particle is coated with 40 ng of TNF.[26] The second group consisted of freshly synthesized and PEGylated GNPs in our lab (F-GNP and F-GNP$^-$). All four GNPs are 30 nm in core diameter and PEGylated with 5 kDa PEG. Table 1 and Supplementary Table T1 in the Supporting Information summarize the technical details for these particles. F-GNP and F-GNP$^-$ were synthesized with a modification of the Frens method.[41] Briefly, 1% sodium citrate (Sigma-Aldrich) was used to synthesize 15 nm gold seed particles by boiling gold chloride (Sigma-Aldrich). A reduction by hydroquinone was used to synthesize 30 nm particles from the 15 nm seeds. The 30 nm GNPs were then incubated with excess PEG5000-thiol (SH-PEG-CH3 or SH-PEG-COOH) (Laysan Bio, Inc., Arab, AL) for 1 h at 60 °C to ensure surface saturation with PEG. The particles were washed 3× to remove any unbound PEG and were characterized for size, charge, and aggregation by DLS, zeta potential, TEM, and UV−vis spectroscopy.

Tumor Cell Implantation and GNP Treatment. All animal experiments were carried out under the NIH guidelines for animal care and were approved by the University of Minnesota Institutional Animal Care and Use Committee. Hindlimb tumor implantation was performed as described previously.[18,42] Briefly, 2−3 × 10^6 LNCaP (human prostate cancer) cells were subcutaneously injected in the hind limb of athymic nude mice (5−6 weeks old). Experiments were performed after 4−5 weeks when a tumor diameter of ∼8 mm was obtained. Animals meeting the criterion for tumor size were randomized in four groups based on four GNP types. Mice were administered intravenously in the tail vein with a single dose of GNPs at 11 mg of Au/kg. This dose was determined based on the TNF dose used in our previous study.[18] Blood and other organs were collected at selected time points. Each group contained at least n = 5−6 animals. The control group did not receive any GNP treatment.

For plasma sensitized GNP (p-GNP) experiment, F-GNP and F-GNP$^-$ were incubated with mouse plasma (isolated from tumor bearing nude mouse) for 1 h at 37 °C. GNPs were then centrifuged and washed with DI water twice to remove any unbound plasma proteins. Thus sensitized p-GNPs were injected at the same dose intravenously as described above.

Blood Distribution. Blood collection from mice was performed via cardiac puncture after CO_2 asphyxiation. Blood fractionation or centrifugation of the whole anticoagulated blood was performed to obtain platelet rich plasma (PRP) and WBCs in a buffy coat. Blood from the untreated mice was centrifuged at 800 rpm for 20 min for the isolation of platelet rich plasma (PRP). PRP is the top, cloudy layer in the centrifuged blood. Blood from the GNP treated mice was centrifuged at 3500 rpm for 20 min for plasma and buffy coat isolation. Buffy coat is the second layer remaining after the removal of the top layer of plasma and contains white blood cells.

Transmission Electron Microscopy. In Vitro GNP Uptake by Platelets. PRP was washed twice in citrate-citric-dextrose (CCD) buffer (93 mM sodium citrate; 7 mM citric acid; 140 mM dextrose; 3 mM theophylline; 5 mM adenosine; pH 6.5) at 2000 rpm for 5 min. Platelets remaining in the pellet were resuspended in Hanks buffer (Invitrogen) and incubated at 37 °C for 20 min. A drop of platelet solution was placed on a TEM grid to allow platelet attachment for 30 min at 37 °C. The grid was then washed gently with Hanks buffer and incubated with GNPs by placing a drop of GNPs (0.15 nM) on the grid for 15 min. At the end of the incubation period, platelets (on the grids) were fixed in 2% glutaraldehyde, washed in DI water, and allowed to air-dry.

In Vivo GNP Uptake by White Blood Cells. After centrifugation, plasma was carefully aspirated from the 1.5 mL centrifuge tube and the buffy coat was gently washed in the tube with 1% glutaraldehyde/white saline.[43] A 3% glutaralde-

hyde solution was gently placed on top of the buffy coat, and fixation was allowed for 20−30 min. When the buffy coat was stiff, it was excised from the tube and cut into 1 mm^3 blocks, which were further allowed to fix for 2 h. The blocks were postfixed in a 1% osmium tetroxide/1.5% potassium ferrocyanide mixture for 1 h and dehydrated in graded concentrations of ethanol and propylene oxide. Samples were then embedded in Epon (Polysciences Inc., Warrington, PA) and sectioned. Thin sections (60−70 nm) were collected on Formvar coated 200 mesh copper grids (Ted Pella, Inc., Redding, CA) and stained with uranyl acetate and lead citrate. This method of fixation allowed simultaneous viewing of platelets, WBCs, and RBCs on the same section.

All grids were visualized under a transmission electron microscope (JEOL 1200 EXII, Hitachi, Japan).

Quantification of Au in Blood by ICP-MS. Whole blood samples were kept frozen until ready for analysis. Blood samples were thawed and vortexed to obtain homogeneous samples. Gold quantification was performed using a Perkin-Elmer Elan 6000 and DRC II inductively coupled plasma mass spectrometer (ICP-MS). Each sample was diluted 1:1 with 0.5% nitric acid. Before analysis 200 μL of sample was diluted 25:1 with 5 mL of 0.5% nitric acid containing 10 ppb bismuth as an internal standard. A six-point calibration curve spanning known gold concentrations of 20−1000 ng/mL and the quantitation was performed by linear regression of the measured intensity of the analyte and internal standard versus the concentration of the calibration standards. All calculated results were reported in nanograms of gold per milliliter of sample. The theoretical detection limit for ICP-MS is 0.02 μg/mL.

Complement Activation ELISA. Platelet poor plasma was collected from fresh blood of treated animals and was stored at −80 °C until further use after addition of Futhan (Sigma-Aldrich). A standard sandwich ELISA with rat anti-mouse C3a capture and detection antibodies (BD Pharmingen) was used. Briefly, ELISA plates were coated with capture antibodies overnight (1:500 in coating buffer) at 4 °C. The plates were washed and blocked with assay diluents. Samples (and standards) were diluted 100× and incubated at room temperature for 2 h. After five washing steps, 100 μL of working detection solution (biotinylated detection Ab and streptavidin−HRP) was added to the wells. After 1 h incubation and seven wash steps, the wells were incubated with color substrate (R&D systems) in the dark for 30 min. After addition of stop solution, the detection was performed at 450 nm in a plate reader.

Tissue Biodistribution. *Histology for GNP Tissue Distribution.* Tumor, liver, and spleen tissues from at least 3 animals per group were formalin fixed, dehydrated in ethanol, and embedded in paraffin. Sections (3 μm thickness) from each tissue were collected on two glass slides. Deparaffinized sections underwent silver enhancement procedure, which selectively precipitates silver onto gold so that it can be visualized under light microscopy. Briefly, deparaffinized sections were washed in DI water, 0.02 M sodium citrate (pH 3.5), and DI water in that order. Sections were silver enhanced using LI Silver (Nanoprobes, Inc., Yaphank, NY) and counterstained with hematoxylin and eosin (H&E).

ICP-AES for Au Quantification. Gold quantification in tissues was performed using a Perkin-Elmer Optima 3000DV atomic emission spectrometer as described previously.[18] Briefly, about 0.2−0.3 g of each tissue (tumor, liver, and spleen) was digested in 2−5 mL of aqua regia (4 parts concentrated HNO_3 + 1 part concentrated HCl). At least 3−6 animals were used for each data point. Before analysis, each sample was diluted 1:1 with a solution of 2 ppm yttrium in dilute nitric acid as an internal standard. Calibration of the instrument was performed using a solution of 1 ppm gold and 1 ppm yttrium in 50% aqua regia. Aliquots of this solution were analyzed by comparing them to a calibration curve constructed using multielement standards. Organ Au concentrations were normalized to total tissue weight. The theoretical detection limit for ICP-AES is 200 μg/mL.

■ ASSOCIATED CONTENT

Ⓢ Supporting Information

Additional GNP characterization data and supporting TEM. This material is available free of charge via the Internet at http://pubs.acs.org.

■ AUTHOR INFORMATION

Corresponding Author

*Corresponding Author: John C. Bischof, Professor Department of Mechanical Engineering University of Minnesota 111 Church Street SE Minneapolis, MN 55455, USA Phone: +1-612-625-5513, Fax: +1-612-625-4344, E-mail: bischof@umn.edu.

Notes

The authors declare no competing financial interest.

■ ACKNOWLEDGMENTS

The authors wish to thank Dr. Steve Schmechel for useful discussions and guidance for the histology work. We thank Carl Walkey and Warren Chan (University of Toronto), Colleen Forster, and Marcy Krumweide for technical support. Parts of this work were carried out in the Characterization Facility, University of Minnesota, which receives partial support from NSF through the MRSEC program. L-GNP and L-GNP^{TNF} were gifts from CytImmune Sciences (Rockville, MD). Part of this project was supported by award number F31GM092259 (to N.B.S.) from the National Institute of General Medical Sciences, and a Distinguished McKnight University Professorship at University of Minnesota (to J.C.B.).

■ REFERENCES

(1) Kim, B. Y. S.; Rutka, J. T.; Chan, W. C. W. Nanomedicine. *N. Engl. J. Med.* **2010**, *363* (25), 2434−2443.

(2) Cytimmune. http://www.cytimmune.com/go.cfm?do=Page.View&pid=26. 2009.

(3) Nanospectra. http://www.nanospectra.com/technology/aurolasetherapy.html. 2009.

(4) Libutti, S. K.; Paciotti, G. F.; Byrnes, A. A.; Alexander, H. R., Jr.; Gannon, W. E.; Walker, M.; Seidel, G. D.; Yuldasheva, N.; Tamarkin, L. Phase I and pharmacokinetic studies of CYT-6091, a novel PEGylated colloidal gold-rhTNF nanomedicine. *Clin. Cancer Res.* **2010**, *16* (24), 6139−6149.

(5) Khlebtsov, N.; Dykman, L. Biodistribution and toxicity of engineered gold nanoparticles: a review of in vitro and in vivo studies. *Chem. Soc. Rev.* **2011**, *40*, 1647−1671.

(6) Zhang, X. D.; Wu, H. Y.; Wu, D.; Wang, Y. Y.; Chang, J. H.; Zhai, Z. B.; Meng, A. M.; Liu, P. X.; Zhang, L. A.; Fan, F. Y. Toxicologic effects of gold nanoparticles in vivo by different administration routes. *Int. J. Nanomed.* **2010**, *5*, 771−781.

(7) Lasagna-Reeves, C.; Gonzalez-Romero, D.; Barria, M. A.; Olmedo, I.; Clos, A.; Sadagopa Ramanujam, V. M.; Urayama, A.; Vergara, L.; Kogan, M. J.; Soto, C. Bioaccumulation and toxicity of

gold nanoparticles after repeated administration in mice. *Biochem. Biophys. Res. Commun.* **2010**, *393* (4), 649−655.
(8) Glazer, E. S.; Zhu, C.; Hamir, A. N.; Borne, A.; Thompson, C. S.; Curley, S. A. Biodistribution and acute toxicity of naked gold nanoparticles in a rabbit hepatic tumor model. *Nanotoxicology* **2011**, *5* (4), 459−468.
(9) Drummond, D. C.; Meyer, O.; Hong, K.; Kirpotin, D. B.; Papahadjopoulos, D. Optimizing liposomes for delivery of chemotherapeutic agents to solid tumors. *Pharmacol. Rev.* **1999**, *51* (4), 691−743.
(10) Moghimi, S. M.; Hunter, A. C.; Murray, J. C. Long-Circulating and Target-Specific Nanoparticles: Theory to Practice. *Pharmacol. Rev.* **2001**, *53* (2), 283−318.
(11) Nie, S. Understanding and overcoming major barriers in cancer nanomedicine. *Nanomedicine* **2010**, *5* (4), 523−528.
(12) Perrault, S. D.; Walkey, C.; Jennings, T.; Fischer, H. C.; Chan, W. C. W. Mediating Tumor Targeting Efficiency of Nanoparticles Through Design. *Nano Lett.* **2009**, *9* (5), 1909−1915.
(13) Bartneck, M.; Keul, H. A.; Singh, S.; Czaja, K.; Bornemann, J.; Bockstaller, M.; Moeller, M.; Zwadlo-Klarwasser, G.; Groll, J. Rapid Uptake of Gold Nanorods by Primary Human Blood Phagocytes and Immunomodulatory Effects of Surface Chemistry. *ACS Nano* **2010**, *4* (6), 3073−3086.
(14) Cho, W.-S.; Cho, M.; Jeong, J.; Choi, M.; Han, B. S.; Shin, H.-S.; Hong, J.; Chung, B. H.; Jeong, J.; Cho, M.-H. Size-dependent tissue kinetics of PEG-coated gold nanoparticles. *Toxicol. Appl. Pharmacol.* **2010**, *245* (1), 116−123.
(15) Choi, C. H. J.; Alabi, C. A.; Webster, P.; Davis, M. E. Mechanism of active targeting in solid tumors with transferrin-containing gold nanoparticles. *Proc. Natl. Acad. Sci. U.S.A.* **2010**, *107* (3), 1235−1240.
(16) Huang, X.; Peng, X.; Wang, Y.; Wang, Y.; Shin, D. M.; El-Sayed, M. A.; Nie, S. A Reexamination of Active and Passive Tumor Targeting by Using Rod-Shaped Gold Nanocrystals and Covalently Conjugated Peptide Ligands. *ACS Nano* **2010**, *4* (10), 5887−5896.
(17) Hardonk, M. J.; Harms, G.; Koudstaal, J. Zonal heterogeneity of rat hepatocytes in the in vivo uptake of 17 nm colloidal gold granules. *Histochemistry* **1985**, *83* (5), 473−477.
(18) Goel, R.; Shah, N.; Visaria, R.; Paciotti, G. F.; Bischof, J. C. Biodistribution of TNF-alpha coated gold nanoparticles in an in vivo model system. *Nanomedicine* **2009**, *4* (4), 401−410.
(19) Dobrovolskaia, M. A.; Patri, A. K.; Zheng, J.; Clogston, J. D.; Ayub, N.; Aggarwal, P.; Neun, B. W.; Hall, J. B.; McNeil, S. E. Interaction of colloidal gold nanoparticles with human blood: effects on particle size and analysis of plasma protein binding profiles. *Nanomed.: Nanotechnol., Biol. Med.* **2009**, *5* (2), 106−117.
(20) Gref, R.; Lück, M.; Quellec, P.; Marchand, M.; Dellacherie, E.; Harnisch, S.; Blunk, T.; Müller, R. H. "Stealth" corona-core nanoparticles surface modified by polyethylene glycol (PEG): influences of the corona (PEG chain length and surface density) and of the core composition on phagocytic uptake and plasma protein adsorption. *Colloids Surf., B* **2000**, *18* (3−4), 301−313.
(21) Malmsten, M.; Emoto, K.; Van Alstine, J. M. Effect of Chain Density on Inhibition of Protein Adsorption by Poly(ethylene glycol) Based Coatings. *J. Colloid Interface Sci.* **1998**, *202* (2), 507−517.
(22) Zhang, D.; Neumann, O.; Wang, H.; Yuwono, V. M.; Barhoumi, A.; Perham, M.; Hartgerink, J. D.; Wittung-Stafshede, P.; Halas, N. J. Gold Nanoparticles Can Induce the Formation of Protein-based Aggregates at Physiological pH. *Nano Lett.* **2009**, *9* (2), 666−671.
(23) Zeineldin, R.; Al-Haik, M.; Hudson, L. G. Role of Polyethylene Glycol Integrity in Specific Receptor Targeting of Carbon Nanotubes to Cancer Cells. *Nano Lett.* **2009**, *9* (2), 751−757.
(24) Moghimi, S. M.; Patel, H. M. Serum-mediated recognition of liposomes by phagocytic cells of the reticuloendothelial system—The concept of tissue specificity. *Adv. Drug Delivery Rev.* **1998**, *32* (1−2), 45.
(25) Deng, Z. J.; Liang, M.; Monteiro, M.; Toth, I.; Minchin, R. F. Nanoparticle-induced unfolding of fibrinogen promotes Mac-1 receptor activation and inflammation. *Nat. Nano* **2010**, *6* (1), 39−44.
(26) Paciotti, G. F.; Myer, L.; Weinreich, D.; Goia, D.; Pavel, N.; McLaughlin, R. E.; Tamarkin, L. Colloidal Gold: A Novel Nanoparticle Vector for Tumor Directed Drug Delivery. *Drug Delivery* **2004**, *11* (3), 169−183.
(27) Dan, N.; Tirrell, M. Polymers tethered to curves interfaces: a self-consistent-field analysis. *Macromolecules* **1992**, *25* (11), 2890−2895.
(28) Lunov, O.; Syrovets, T.; Loos, C.; Beil, J.; Delacher, M.; Tron, K.; Nienhaus, G. U.; Musyanovych, A.; Mailänder, V.; Landfester, K.; Simmet, T. Differential Uptake of Functionalized Polystyrene Nanoparticles by Human Macrophages and a Monocytic Cell Line. *ACS Nano* **2011**, *5* (3), 1657−1659.
(29) Bartneck, M.; Keul, H. A.; Zwadlo-Klarwasser, G.; Groll, J. Phagocytosis Independent Extracellular Nanoparticle Clearance by Human Immune Cells. *Nano Lett.* **2009**, *10* (1), 59−63.
(30) White, J. G.; Clawson, C. C. The surface-connected canalicular system of blood platelets—a fenestrated membrane system. *Am. J. Pathol.* **1980**, *101* (2), 353−364.
(31) White, J. G. Platelets are covercytes, not phagocytes: uptake of bacteria involves channels of the open canalicular system. *Platelets* **2005**, *16* (2), 121−131.
(32) Movat, H. Z.; Weiser, W. J.; Glynn, M. F.; Mustard, J. F. Platelet phagocytosis and aggregation. *J. Cell Biol.* **1965**, *27* (3), 531−543.
(33) Chambers, E.; Mitragotri, S. Prolonged circulation of large polymeric nanoparticles by non-covalent adsorption on erythrocytes. *J. Controlled Release* **2004**, *100* (1), 111−119.
(34) Hall, S. S.; Mitragotri, S.; Daugherty, P. S. Identification of Peptide Ligands Facilitating Nanoparticle Attachment to Erythrocytes. *Biotechnol. Prog.* **2007**, *23* (3), 749−754.
(35) Zhao, Y.; Sun, X.; Zhang, G.; Trewyn, B. G.; Slowing, I. I.; Lin, V. S. Y. Interaction of Mesoporous Silica Nanoparticles with Human Red Blood Cell Membranes: Size and Surface Effects. *ACS Nano* **2011**, *5* (2), 1366−1375.
(36) Rothen-Rutishauser, B. M.; Schurch, S.; Haenni, B.; Kapp, N.; Gehr, P. Interaction of fine particles and nanoparticles with red blood cells visualized with advanced microscopic techniques. *Environ. Sci. Technol.* **2006**, *40* (14), 4353−4359.
(37) van Horssen, R.; Ten Hagen, T. L.; Eggermont, A. M. TNF-alpha in cancer treatment: molecular insights, antitumor effects, and clinical utility. *Oncologist* **2006**, *11* (4), 397−408.
(38) Farma, J. M.; Puhlmann, M.; Soriano, P. A.; Cox, D.; Paciotti, G. F.; Tamarkin, L.; Alexander, H. R. Direct evidence for rapid and selective induction of tumor neovascular permeability by tumor necrosis factor and a novel derivative, colloidal gold bound tumor necrosis factor. *Int. J. Cancer* **2007**, *120* (11), 2474−2480.
(39) Franke, H.; Durer, U.; Schlag, B.; Dargel, R. In vivo binding and uptake of low-density lipoprotein-gold- and albumin-gold conjugates by parenchymal and sinusoidal cells of the fetal rat liver. *Cell Tissue Res.* **1987**, *249* (1), 221−226.
(40) Leenen, P. J. M.; Radosevic, K.; Voerman, J. S. A.; Salomon, B. t.; van Rooijen, N.; Klatzmann, D.; van Ewijk, W. Heterogeneity of Mouse Spleen Dendritic Cells: In Vivo Phagocytic Activity, Expression of Macrophage Markers, and Subpopulation Turnover. *J. Immunol.* **1998**, *160* (5), 2166−2173.
(41) Frens, G. Controlled nucleation for the regulation of the particle size in monodisperse gold suspensions. *Nat. Phys. Sci.* **1973**, *241* (105), 20.
(42) Goel, R.; Swanlund, D.; Coad, J.; Paciotti, G. F.; Bischof, J. C. TNF-alpha-based accentuation in cryoinjury—dose, delivery, and response. *Mol. Cancer Ther.* **2007**, *6* (7), 2039−2047.
(43) White, J. G. Interaction of membrane systems in blood platelets. *Am. J. Pathol.* **1972**, *66* (2), 295−312.